Interaction of Sulforaphane with DNA and RNA

Farzaneh Abassi Joozdani[1], Faramarz Yari[1], Parvaneh Abassi Joozdani[1], Shohreh Nafisi[2,3]*

1 Department of Biology, IAU, Science and Research Branch, Tehran, Iran, **2** Department of Chemistry, IAU, Central Tehran Branch, Tehran, Iran, **3** Department of Dermatology, University of California, San Francisco, California, United States of America

* drshnafisi@gmail.com

Abstract

Sulforaphane (SFN) is an isothiocyanate found in cruciferous vegetables with anti-inflammatory, anti-oxidant and anti-cancer activities. However, the antioxidant and anticancer mechanism of sulforaphane is not well understood. In the present research, we reported binding modes, binding constants and stability of SFN–DNA and -RNA complexes by Fourier transform infrared (FTIR) and UV–Visible spectroscopic methods. Spectroscopic evidence showed DNA intercalation with some degree of groove binding. SFN binds minor and major grooves of DNA and backbone phosphate (PO_2), while RNA binding is through G, U, A bases with some degree of SFN–phosphate (PO_2) interaction. Overall binding constants were estimated to be $K_{(SFN–DNA)}=3.01$ (± 0.035)$\times10^4$ M^{-1} and $K_{(SFN–RNA)}= 6.63$ (±0.042)$\times10^3$ M^{-1}. At high SFN concentration (SFN/RNA = 1/1), DNA conformation changed from B to A occurred, while RNA remained in A-family structure.

Introduction

Sulforaphane (1-isothiocyanato-4-(methyl-sulfinyl)) butane, a molecule within the isothiocyanate group of organosulfur compounds (Fig 1); is the most characterized isothiocyanate found at high levels in cruciferous vegetables such as broccoli, cabbages, kale, Brussels sprouts, radish, and mustard [1]. It has shown anti-inflammatory, antibiotic, antioxidant and anticarcinogenic properties [2–10]. Sulforaphane chemoprevention properties against cancer are through both "blocking" and "suppressing" effects [11]. Blocking function is inhibiting Phase 1 metabolism enzymes which can activate procarcinogenic compounds to their carcinogenic metabolites and induce phase 2 metabolic enzymes. Suppressing effects revealed modulating diverse cellular activities and inhibiting growth of transformed cells [11, 12]. SFN acts as an antioxidant by increasing reduced glutathione levels as well as inducing cell cycle arrest and apoptosis [13, 14] by regulation of many molecules including Bcl-2 family proteins, caspases, p21, cyclins and cdks [12, 13]. Gene expression of phase 2 proteins is regulated by three cellular components; Kelch-like ECH-associated protein 1 (Keap 1); Nuclear factor (eryhthroid-derived 2)-like 2 (Nrf2); and ARE (anti-oxidant response element). Under normal conditions, Nrf2 is
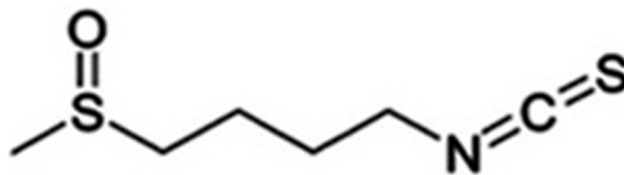
Fig 1. Chemical structure of sulforaphane (SFN).

sequestered in cytoplasm by Keap 1 and is subject to ubiquitination and proteasomal degradation. In the presence of SFN, it targets and chemically modifies specific and highly reactive cysteine thiols of Keap 1 resulting conformational changes and dissociation of Nrf2 from Keap 1, and stabilization of Nrf2. Nrf2 undergoes nuclear translocation and binds to ARE and activates transcription of phase 2 genes [15– 21].

Even though much is reported about antitumor activities of sulforaphane, there has been no report on the molecular aspects of sulforaphane interaction with DNA and RNA in aqueous solution. RNA, a versatile molecule playing essential roles in many biological processes is an attractive target for potential therapeutics. Recent progress in antiviral research has been mainly based on targeting RNA molecules for therapeutic intervention. Development of molecules capable of controlling RNA activity is now a focus of medicinal and chemico-biological research [22–24]. Understanding the mechanism of sulforaphane action may expedite development of new drugs based on SFN. So far, little is known about sulforaphane interaction with individual DNA and RNA. Thus, we compared SFN interaction with DNA and RNA in aqueous solution at pH 6.5–7.5 with sulforaphane / DNA, RNA (P) molar ratios of 1/80 to1/1 by FTIR and UV measurements. Structural analyses regarding drug binding site, binding constant, and DNA, RNA secondary structures are presented here. Our spectroscopic results provided structural analysis of sulforaphane—biopolymer interactions.

Materials and Methods

Materials

DNA sodium salt, and Baker's yeast RNA sodium sulforaphane were purchased from Sigma Chemical (St. Louis, MO) and used without further purification. To check the protein content of DNA and RNA solutions, the absorbance bands at 258 and 280 nm were used. The A_{258}/A_{280} ratio was 1.80 for DNA and A_{260}/A_{280} ratio 2.10 for RNA, showing that DNA and RNA samples were sufficiently free from protein [25]. Other chemicals were of reagent grade and used without further purification.

Preparation of stock solutions. Sodium–DNA or sodium–RNA were dissolved to 0.5% w/v (0.0125M (phosphate)) in NaCl (0.1 M) solution for 24 h with occasional stirring to ensure the formation of a homogeneous solution. The final concentration of the calf thymus DNA and yeast RNA solution were determined spectrophotometrically at 258 nm using molar extinction coefficient $\varepsilon_{259} = 6600$ cm^{-1} M^{-1} (DNA) and $\varepsilon_{258} = 9250$ cm^{-1} M^{-1} (RNA) (expressed as molarity of the phosphate groups) [26]. The definite amounts of sulforaphane (0.05–12.5 mM) were dissolved in water and added dropwise to biopolymers solutions (12.5mM) to attain the desired drug/DNA and RNA (P) molar ratios (r) of 1/80, 1/40, 1/20, 1/10, 1/5 and 1/1 with a final DNA (P) and RNA concentrations of 6.25 mM. At higher concentrations of sulforaphane /RNA (r = 1/1), the experiments could not be continued due to DNA gel formation. The pH values of the solutions were adjusted at 7.0±0.2 using NaOH solution. The infrared spectra were recorded 1h after mixing of the drugs with DNA or RNA solution. For UV measurements,

the drug concentrations of 5×10^{-6}–1×10^{-4} M were used with constant DNA or RNA concentration of 5×10^{-4} M.

FTIR spectroscopy measurements

Infrared spectra were recorded on a Nicolet FTIR spectrometer (Magna 550) equipped with a liquid-nitrogen-cooled HgCdTe (MCT) detector. The spectra of drugs/DNA or drug/RNA solutions were taken using a cell assembled with ZnSe windows. Spectra were collected and treated using the OMNIC software supplied by the manufacturer of the spectrophotometer. The spectra of the solutions were recorded after 1h incubation of drugs with DNA or RNA solutions. The bands were measured in triplicates (three individual samples of the same DNA or RNA and drug concentrations). For each spectrum, 100 scans were collected with resolution of $4\ cm^{-1}$. The difference spectra [(polynucleotide solution+ drug solution)-(polynucleotide solution)] were obtained using a sharp DNA and RNA band at $968\ cm^{-1}$ as internal reference [27,28]. This band, which is due to sugar C-C and C-O stretching vibrations, exhibits no spectral change (shifting or intensity variation) upon drug–DNA,—RNA complexation, and is cancelled out upon spectral subtraction.

The intensity ratios of the bands due to several DNA in-plane vibrations related to A-T and G-C base pairs and RNA in-plane vibrations related to A-U and G-C base pairs and the phosphate stretching vibrations were measured with respect to the reference bands at $968\ cm^{-1}$ (DNA and RNA) as a function of sulforaphane concentrations with an error of ±3%. Similar intensity variations have been used to determine the ligand binding to DNA and RNA bases and backbone phosphate groups [29]. The plots of the relative intensity (R) of several peaks of DNA in-plane vibrations related to A-T and G-C base pairs and the phosphate stretching vibrations such as 1714 (guanine), 1665 (thymine), 1610 (adenine), 1490 (cytosine), 1226 (asymmetric PO_2), and $1088\ cm^{-1}$ (symmetric PO_2) and RNA in-plane vibrations related to A-U and G-C base pairs and the phosphate stretching vibrations such as 1697 (guanine), 1650 (uracil), 1610 (adenine), 1488 (cytosine), and $1241cm^{-1}$ (phosphate groups) versus sulforaphane concentrations were obtained after peak normalization using $R_i = I_i/I_{968}$, where I_i is the intensity of the absorption peak for pure DNA or RNA in the complex with i as ligand concentration, and I_{968} is the intensity of the $968\ cm^{-1}$ peak (DNA and RNA internal reference) (Fig 2A and 2B).

Absorption spectroscopy

The absorption spectra were recorded on a LKB model T90 + UV/Vis Spectrometer PG Instruments ltd, quartz cuvettes of 1cm were used and the absorption spectra recorded with drug concentrations of 5×10^{-6}–1×10^{-4} M and constant polynucleotide concentration of 5×10^{-4} M.

The binding constants of the drug-DNA or drug-RNA complexes were calculated as reported [30]. It is assumed that the interaction between the drug [L] and the substrate [S] is 1:1; for this reason a single complex SL (1:1) is formed. The relationship between the observed absorbance change per centimeter and the system variables and parameters is as follow;

$$\frac{\Delta A}{b} = \frac{S_t K_{11} \Delta\varepsilon_{11}[L]}{1 + K_{11}[L]}$$

1

where $\Delta A = A—A_0$ from the mass balance expression $S_t = [S] + [SL]$, we get

$[S] = S_t/(1 + K_{11}[L])$. Eq (1) is the binding isotherm, which shows the hyperbolic

dependence on free ligand concentration. The double-reciprocal form of plotting the rectangular hyperbola $\frac{1}{y} = \frac{f}{d} \cdot \frac{1}{x} + \frac{e}{d}$, is based on the linearization of Eq (1) according to the following
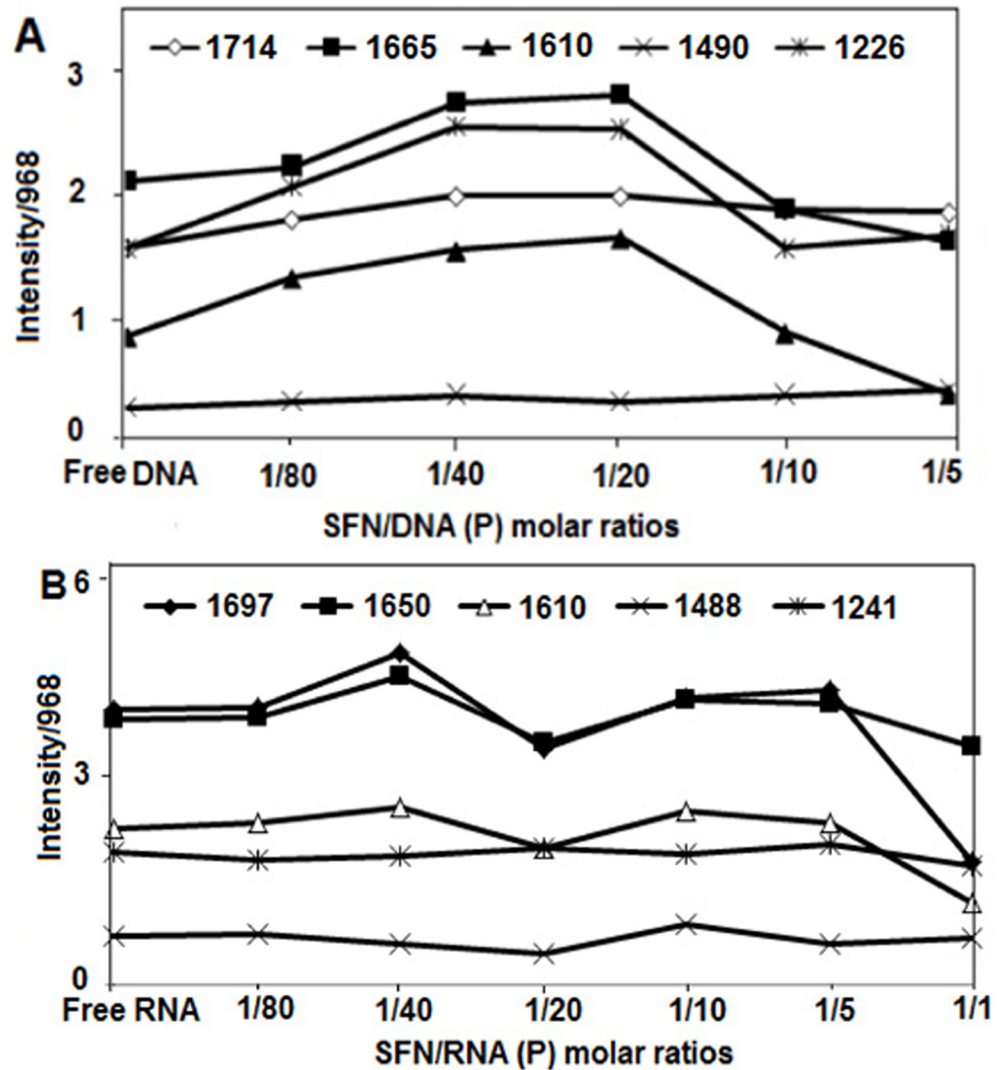
Fig 2. Intensity ratio variations for several DNA and RNA in-plane vibrations as a function of SFN concentration. (A) Intensity ratios for DNA bands at 1714 (G, T), 1665 (T, G, A, C), 1610 (A), 1490 (C,G) and 1226 (PO2 asymmetric) referenced to the DNA band at 966 cm^{-1}. (B) Intensity ratios for the RNA bands at 1697 (G, U), 1650 (U, G, A, C), 1610 (A), 1488 (C,G) and 1241 (PO2 asymmetric) referenced to the RNA band at 969 cm^{-1}.

doi:10.1371/journal.pone.0127541.g002

equation,

$$\frac{b}{\Delta A} = \frac{1}{S_t K_{11} \Delta \varepsilon_{11} [L]} + \frac{1}{S_t \Delta \varepsilon_{11}} \qquad 2$$

Thus the double reciprocal plot of $1/\Delta A$ versus $1/[L]$ is linear and the binding constant can be estimated from the following equation:

$$K_{11} = \frac{intercept}{slope} \qquad 3$$

Molecular modeling and docking

The crystal structures of two DNA–drug and RNA-drug complexes were selected from Protein Data Bank (Web address: http://www.rcsb.org) PDB ID: 1BNA-DNA and PDB ID: 2R22 and PDB ID:3CZW [31]. The crystal structure of the synthetic DNA dodecamer d(CpGpCpGpApApTpTpCpGpCpG) has been used for simulation. Sulforaphane docked onto the DNA and RNA from the crystal structures. For every individual model, the correlation between calculated binding and experimental values were analyzed to determine the most representative model. To determine the preferred the binding sites on DNA, docking studies were performed by AutoDock 4.0.1 software ([32]; Web address: http://autodock.scripps.edu). The sulforaphane structure was extracted from Pubchem (CID 16213697,10114) file. In order to use the structures for docking, the universal force field (for drugs) [33] and Merck molecular force field 94 (for macromolecule) [34] were short minimized. Docking to macromolecule was carried out using the Lamarckian genetics algorithm. For the local search, the so-called pseudo-Solis and Wets algorithm was applied using a maximum of 300 iterations per local search [35]. In Auto-Dock, the overall docking energy of a given drug molecule in its active site is expressed as follows:

$$\Delta G = \Delta G_{vdW} \sum_{i,j} \left(\frac{A_{ij}}{r_{ij}^{12}} - \frac{B_{ij}}{r_{ij}^{6}} \right) + \Delta G_{hbond} \sum_{i,j} \left(\frac{C_{ij}}{r_{ij}^{12}} - \frac{D_{ij}}{r_{ij}^{10}} + E_{hbond} \right) + \Delta G_{elec} \sum_{i,j} \frac{q_i - q_j}{\varepsilon(r_{ij}) r_{ij}}$$
$$+ \Delta G_{tor} N_{tor} + \Delta G_{sol} \sum_{i_C, j} S_i V_j e^{(-r_{ij}^2 / 2\sigma^2)} \qquad 4$$

In Eq (4), ΔG_{vdW}, ΔG_{hbond}, ΔG_{elec}, ΔG_{tor}, and ΔG_{sol} are free energy coefficients of van der Waals, hydrogen bond, electrostatic interactions, torsional term, and desolvation energy of oligonucleotide–drug complex, respectively. r_{ij}, A_{ij}, B_{ij}, C_{ij}, and D_{ij} represent the interatomic distance, the depths of energy well, and the equilibrium separations between the two atoms, respectively. The first three terms are in vacuo force field energies for intermolecular interactions. The fourth term accounts for the internal steric energy of the drug molecule. The energies used and reported by AutoDock should be distinguished: there are docked energies, which include the intermolecular and intramolecular interaction energies, and are used during dockings, and predicted free energies, which include the intermolecular energy and the torsional free energy, and are only reported at the end of a docking [36, 37]. We converted between the binding constant, $K_{binding}$ and the binding free energy change of binding, $\Delta G_{binding}$, using the following equation:

$$\Delta G_{binding} = -RT \ln K_{binding} \qquad 5$$

where R is the gas constant, 1.987 cal K^{-1} mol^{-1}, and T is the absolute temperature, assumed to be room temperature, 298.15 K.

In order to analyze and display docking results, we used AutoDock Tools 1.5.4 (ADT) ([38]; Web address: http://mgltools.scripps.edu) and UCSF Chimera 1.6.1([39];Web address: http://www.cgl.ucsf.edu/chimera).

Results and Discussion

Infrared spectra of sulforaphane–DNA complexes

Evidence of sulforaphane–DNA complexation comes from the infrared spectroscopic results shown in Figs 3A and 2A. The spectral changes (intensity and shifting) of several prominent DNA in-plane vibrations at 1714 (G,T; mainly G), 1665 (T, G, A, and C; mainly T), 1610 (A, C;
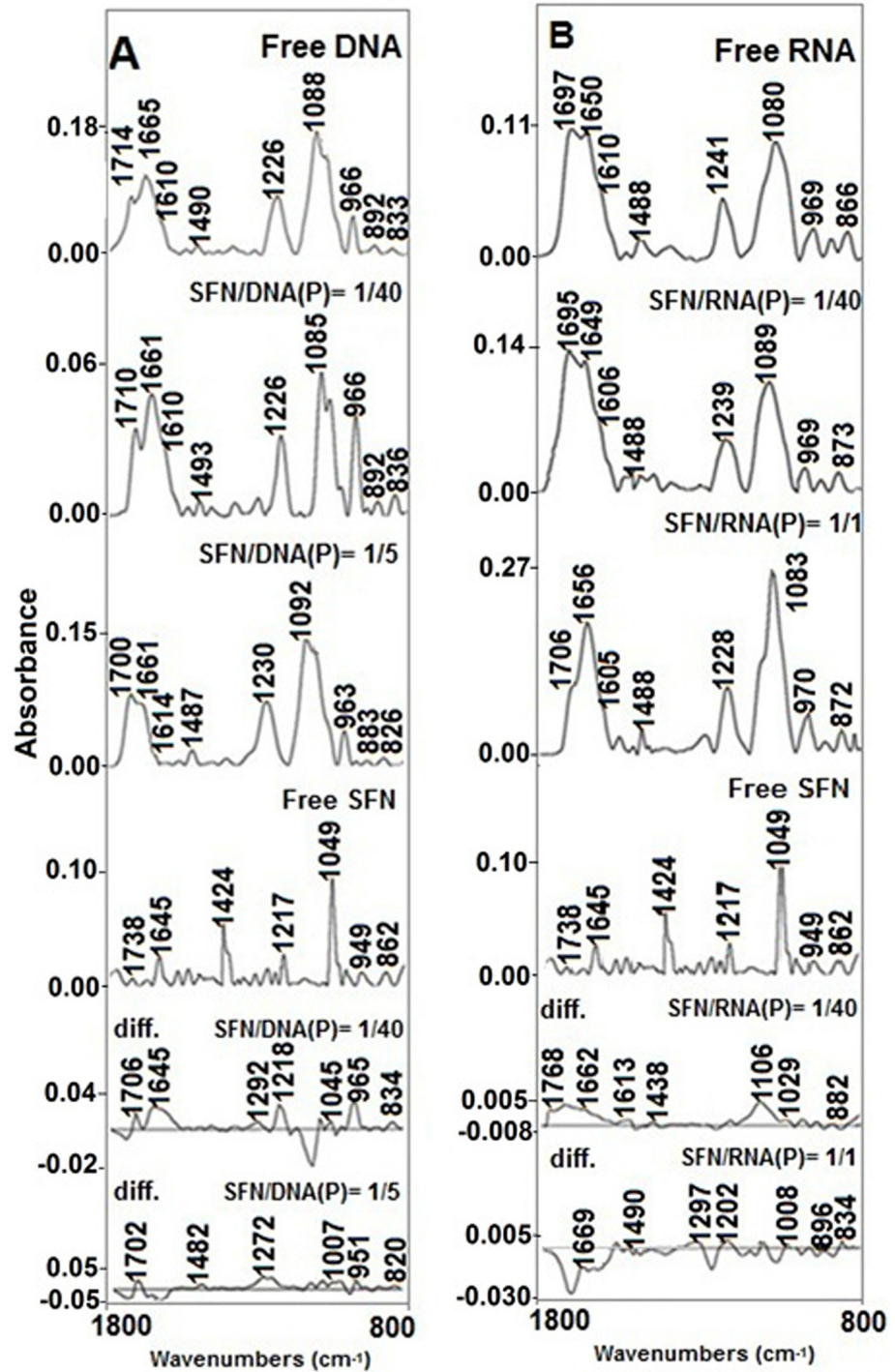
Fig 3. FTIR spectra in the region of 1800–800 cm^{-1} for sulforaphane (SFN), calf thymus DNA (A) and yeast RNA adducts (B) in aqueous solution at pH = 7. DNA or RNA and two complexes spectra were obtained at various SFN/DNA and-RNA (phosphate) molar ratios (three two spectra); sulforaphane and two difference spectra (bottom three spectra).

doi:10.1371/journal.pone.0127541.g003

mainly A), 1490 (C, G; mainly C), 1226 (PO$_2$ asymmetric stretch) and 1088 cm^{-1} (PO$_2$ symmetric stretch) [40–42] were monitored at various SFN concentrations binding to DNA (Fig 3A).

Major interaction was observed with the bases, mainly with minor groove; A-T rich region and guanine of DNA duplex as evidenced by FTIR spectra in Figs 3A and 2A. At low SFN concentrations (r = 1/80 to 1/20), the intensity of the thymine, guanine and adenine bands increased which can be ascribed to the interaction of SFN with bases. At r = 1/10, major decrease in intensity of the bases mainly thymine and adenine and to a lesser extent with guanine can be related to DNA destabilization upon SFN interaction. The observed intensity changes were accompanied by shifting of the guanine band at 1714 to 1710 (r = 1/40) and 1700 cm^{-1} (r = 1/5), thymine band at 1665 to 1661 cm^{-1} (r = 1/40, 1/5), adenine band at 1610 to 1614 cm^{-1} (r = 1/5) (Fig 3A). Major spectral changes (intensity and shifting) of the DNA bases upon sulforaphane interaction is indicative of drastic participation of adenine, thymine and guanine bases in SFN complexation. No major shifting was observed for the cytosine which demonstrated no major participation of cytosine in SFN interaction.

At low SFN concentrations (r = 1/40), no major intensity changes was observed for the phosphate band at 1226 cm^{-1}, however at high concentrations (r = 1/5), it shifted to 1230 cm^{-1} which can be related to phosphate interaction with SFN at higher concentrations (Fig 3A). In addition to major spectral shifting of the PO$_2$ asymmetric band, the relative intensities of the asymmetric (v_{as}) and symmetric (v_s) vibrations were altered upon phosphate interaction [40]. The v_s PO$_2$ (1088 cm^{-1}) and v_{as} PO$_2$ (1226 cm^{-1}) were changed, with the ratio v_s/v_{as} going from 2.16 (free DNA) to 1.95 (SFN–DNA complexes) in various molar ratios of sulforaphane–DNA.

In the difference spectra of sulforaphane-DNA (r = 1/40), the positive features at 1706, 1645, and 1218 cm^{-1} (Fig 3B, Diff. r = 1/40) are due to the intensity increase of the guanine, thymine, and phosphate bands upon sulforaphane complexation and approves major interaction of sulforaphane with guanine N7, thymine O2 and backbone PO$_2$ group.

The UV results indicated intensity increase in the DNA band at 259 nm upon SFN interaction (Fig 4A). Similar spectral changes were observed in other DNA adducts [43]. On the other hand, the UV band at 245 nm characteristic of sulforaphane absorption showed major red shift and appeared at 259 nm upon DNA interaction. The observed major shifting of sulforaphane band is indicative of structural alterations of the SFN upon DNA complexation (Fig 4A).

Infrared spectra of sulforaphane–RNA complexes

Evidence related to sulforaphane-RNA complexation comes from the infrared spectroscopic results shown in Figs 3B and 2B. In the sulforaphane–RNA complexes, SFN binds mainly to guanine and uracil bases and to a lesser extent to adenine bases, as well as the backbone PO$_2$ group (Fig 3B). Evidence for this comes from spectral changes of the bases and phosphate bands upon SFN interaction (Figs 3B and 2B).

No major spectral changes (shifting and intensity) were observed for the bases and phosphate bands at low concentration (r = 1/80). However at r = 1/40, increase in the intensity of guanine, uracil and to a lesser extent adenine bands can be related to sulforaphane interaction with these bases. At r = 1/20, reduction in intensity of the G, U and A bands arise from RNA stabilization upon SFN interaction (Fig 2B). No major interaction was observed for adenine, guanine and uracil bands at higher concentrations (r = 1/10, 1/5) due to minor intensity changes of the bands upon SFN interaction (Fig 2B). At r = 1/1, RNA aggregation occurred upon SFN interaction due to major decrease in intensity of guanine, uracil and adenine bands.

The intensity changes were accompanied by major shifting of the bases bands especially at higher SFN concentrations (r = 1/5); the guanine band at 1697 shifted to 1706 cm^{-1}, the uracil
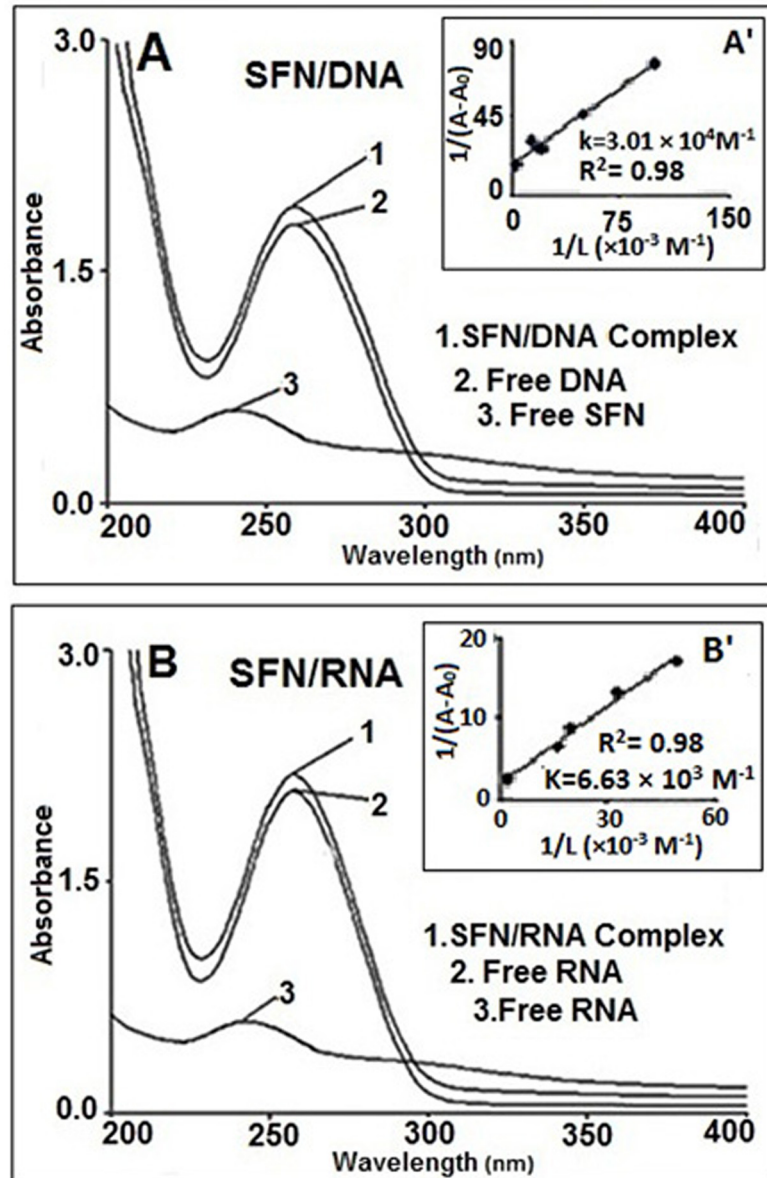
Fig 4. Ultraviolet–visible results of SFN and calf thymus DNA and its Complexes (A), and yeast RNA and its complex (B): (1) SFN–DNA and SFN–RNA complexes; (2) free DNA or free RNA (0.5 mM); (3) free SFN (0.5 mM). Plot of $1/(A-A_0)$ versus (1/drug concentration) for SFN and calf thymus DNA complexes (A$'$), and plot of $1/(A-A_0)$ versus (1/drug concentration) for SFN and yeast RNA complexes (B$'$), where A_0 is the initial absorbance of DNA (259 nm) or RNA at (258 nm) and A is the recorded absorbance at different SFN concentrations (5×10^{-6}–1×10^{-4} M) with constant DNA or RNA concentrations of 0.5 mM at pH 7.

band at 1650 shifted to 1656 cm^{-1}, the adenine band at 1610 shifted to 1605 cm^{-1}. The major spectral changes of RNA bands upon sulforaphane interaction can be related to major interaction of SFN with RNA.

For the backbone PO$_2$ asymmetric stretching, no major shifting was observed at low SFN concentration; 1241 to 1239 cm^{-1} (r = 1/40), however, a drastic shifting was observed at higher concentration; 1241 to 1228 cm^{-1} (r = 1/1) (Fig 2A). Some intensity changes in the backbone phosphate group were also observed upon sulforaphane interaction (r = 1/40 to 1/1). The shifting and
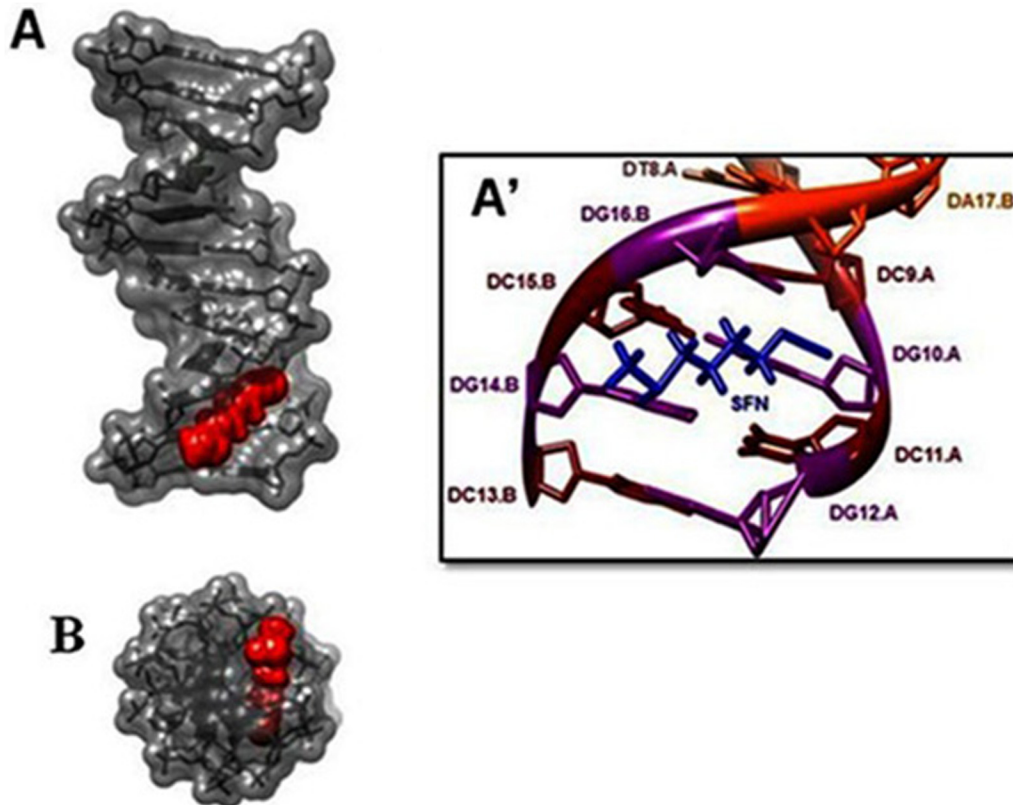
Fig 5. Docking structure between d(CGCGAATTCGCG) (PDB 1BNA-DNA) and SFN. (A) Surface representation of d(CGCGAATTCGCG) complexes with SFN (Display side). (A') Close up view of d(CGCGAATTCGCG) complexes with SFN. (B) Surface representation of d(CGCGAATTCGCG) complexes with SFN (Display top).

intensity changes in the phosphate band upon sulforaphane interaction can be related to the interaction of SFN with phosphate backbone group especially at higher concentrations (Fig 2B).

It is worth mentioning that minor spectral changes for cytosine band at 1488 cm^{-1} upon sulforaphane interaction with RNA is indicative of minor participation of cytosine in SFN complexation (Figs 3B and 2B). Similar spectral changes were observed in other RNA adducts [44].

In the difference spectra of sulforaphane-RNA (r = 1/40), the positive features at 1768, 1662, and 1106 cm^{-1} (Fig 3B, Diff. r = 1/40) are due to the intensity increase of the guanine, uracil, and phosphate bands upon SFN complexation and approves major interaction of sulforaphane with guanine N7, uracil O2 and backbone PO$_2$ group.

Additional evidence regarding sulforaphane–RNA interaction comes from the UV results. An increase in the intensity of RNA band at 258 nm can be related to the interaction of sulforaphane with RNA (Fig 4B). Similar spectral changes were observed in other RNA adducts [43].

On the other hand, the UV band at 245 nm characteristics of sulforaphane absorption showed major red shift and appeared at 258 nm upon RNA interaction. The observed spectral changes can be indicative of structural alterations of the SFN upon its complexation with RNA (Fig 4B).

DNA and RNA conformation

No alterations of B-DNA structure was observed upon SFN-DNA complexation as a result of no major spectral changes for B-DNA marker bands at 1226 cm^{-1} (PO$_2$ stretch), 1714 cm^{-1}
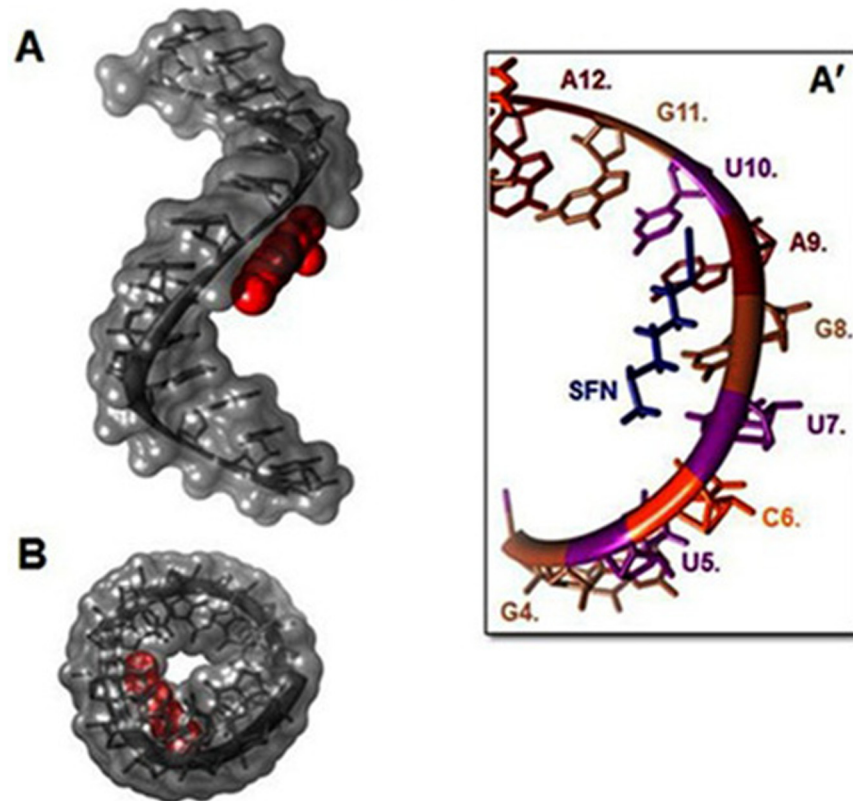
Fig 6. Docking structure between (PDB 3CZW) and SFN. (A) Surface representation of (PDB 3CZW) complexes with SFN (Display side). (A') Close up view of (PDB 3CZW) complexes with SFN. (B) Surface representation of (PDB 3CZW) complexes with SFN (Display top).

(mainly guanine), and 836 cm^{-1} (phosphodiester mode) (Fig 3A). In a B to A transition, the marker band at 836 cm^{-1} shifts toward a lower frequency at about 825–800 cm^{-1}, the guanine band at 1714 cm^{-1} appears at 1700–1695 cm^{-1}, and the phosphate band at 1226 cm^{-1} shifts toward a higher frequency at 1240–1235 cm^{-1} [45–48]. In a B to Z conformational change, the sugar–phosphate band at 836 cm^{-1} appears at 800–780 cm^{-1}, the guanine band displaces to 1690 cm^{-1}, and the phosphate band shifts to 1216 cm^{-1} [47, 48]. In the SFN-DNA complex (r = 1/5), shifting of the B-DNA marker bands at 1714 to 1700 cm^{-1}, at 833 to 826 cm^{-1} and at 1226 to1230 cm^{-1} is indicative of DNA conformational change from B to A upon sulforaphane interaction (Figs 3A and 2A).

In the sulforaphane–RNA complexes, RNA remains in A-conformation. The lack of major shifting of A-RNA marker bands at 1700–1688 (guanine), 1240–1247 (phosphate), 861–867 (ribosephosphate), and 815–809 cm^{-1} (phosphodiester) is indicative of RNA remaining in A-conformation upon sulforaphane complexation (Figs 3B and 2B). [44, 49–51].

Stability of sulforaphane–DNA and sulforaphane–RNA complexes

The sulforaphane–DNA and—RNA binding constants were determined as described in the experimental section (UV–visible spectroscopy). The UV absorption spectra of sulforaphane–DNA and—RNA complexes are shown in Fig 4A and 4B. The calculations of the overall binding constants were carried out using UV spectroscopy as previously reported [30]. Concentrations of the complexed ligand were determined by subtracting absorbance of the free DNA at
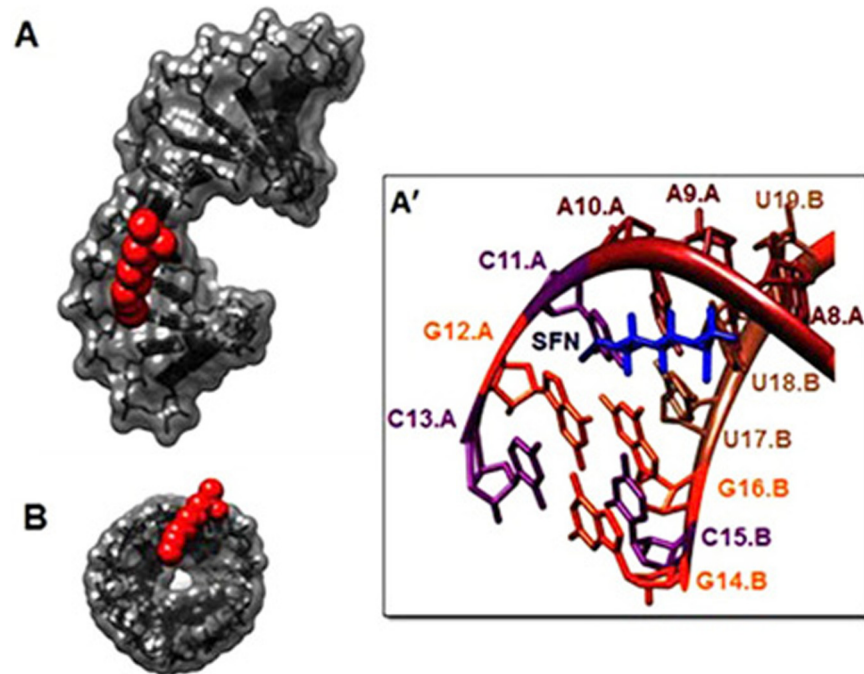
Fig 7. Docking structure between (PDB 2R22) and SFN. (A) Surface representation of (PDB 2R22) complexes with SFN (Display side). (A') Close up view of (PDB 2R22) complexes with SFN. (B) Surface representation of (PDB 2R22) complexes with SFN (Display top).

259 nm and RNA at 258 nm from those of the complexed. Concentration of the free ligand was determined by subtraction of complexed ligand from total ligand used in the experiment. Our data of 1/[ligand complexed] almost proportionally increased as a function of 1/[free ligand] (Fig 4). The double reciprocal plot of $1/(A-A_0)$ versus 1/(sulforaphane concentration) is linear, and the binding constant (K) can be estimated from the ratio of the intercept to the slope (Fig 4), where A_0 is the initial absorbance of the free DNA at 259 nm and free RNA at 258 nm, and A is the recorded absorbance of DNA and RNA in the presence of different sulforaphane concentrations. The overall binding constants are estimated to be $K_{(SFN-DNA)}$ = 3.01 (± 0.035) $\times 10^4$ M^{-1} and $K_{(SFN-RNA)}$ = 6.63 (±0.042) $\times 10^3$ M^{-1}. The affinity of sulforaphane–DNA and—RNA is in the order of SFN–DNA>SFN–RNA. Sulforaphane binding to DNA is stronger, since DNA is double helix, but RNA is not. These binding constants are consistent with FTIR results, which we concluded a stronger interaction of sulforaphane with DNA than that of RNA complexes.

Docking study

Our results from FTIR and UV-Visible spectroscopy are accompanied by docking experiments. In order to determine the preferred binding sites on DNA and RNA, the sulforaphane were docked to DNA and RNA. The dockings results are shown in Figs 5, 6 and 7.

For docking, PDB 3CZW was chosen as single stranded RNA candidate and PDB 2R22 as double stranded RNA candidate. PDB 3CZW and PDB 2R22 include all kinds of bases (A,U,G and C). PDB 1BNA-DNA with minor and major grooves including all kinds of bases (A,T,G and C) was chosen as candidate for double stranded DNA.

The models show that SFN is surrounded by C13.B, G14.B, C15.B, G16.B, C9.A, G10.A, C11.A, G12.A (Fig 5A') and phosphate groups with a binding energy of -4.499 kcal/mol for

DNA. SFN was surrounded by U7, G8, A9, U10 (Fig 6A′) and phosphate groups with a binding energy of -4.41 kcal/mol for single strand RNA. SFN was surrounded by C11.A, A10.A, A9.A, A8.A, G16.B, U17.B, U18.B (Fig 7A′) and phosphate groups with a binding energy of -4.05 kcal/mol for double strand RNA. In several data derived from SFN and 1BNA-DNA, 2R22 and 3CZW the docking shows different mood energy intercalations, the structure was selected which has the most compatibility with FTIR results. Spectroscopic evidence, FTIR and UV results showed both intercalation and external binding of SFN to DNA and RNA. The selected docking data showed perpendicular intercalation into oligonucleotides (1BNA-DNA, 2R22 and 3CZW) (Figs 5A′,6A′ and 7A′).

Conclusion

Our study provided important quantitative data on the binding affinity of sulforaphane to DNA and RNA. Direct binding experiments and DNA denaturation assays need to be done to determine the effect of low and high concentrations of SFN on polynucleotides structure.

We also showed distinct differences in sulforaphane binding to these biopolymers. Interaction of sulforaphane with DNA and RNA can be used to gain insight into the mechanism of action of sulforaphane in cancer therapy. Based on our spectroscopic results and docking studies, the following points are important; sulforaphane binds DNA and RNA *via* both intercalation and groove binding with the order of stability SFN-DNA>SFN-RNA. At high SFN concentrations, DNA conformational changed from B to A occurred, while RNA remained in A-family structure.

Acknowledgments

Author Contributions

Conceived and designed the experiments: FAJ FY PAJ SHN. Performed the experiments: FAJ FY PAJ SHN. Analyzed the data: FAJ FY PAJ SHN. Contributed reagents/materials/analysis tools: FAJ FY PAJ SHN. Wrote the paper: FAJ FY PAJ SHN.

References

1. Zhang Y, Talalay P, Cho CG, Posner GH (1992) A major inducer of anticarcinogenic protective enzymes from broccoli: isolation and elucidation of structure. Proc Natl Acad Sci. 89: 2399–2403. PMID: 1549603

2. Zhang Y, Tang L (2007) Discovery and development of sulforaphane as a cancer chemopreventive phytochemical. Acta Pharmacol Sin. 28: 1343–1354. PMID: 17723168

3. Posner GH, Cho CG, Green JV, Zhang Y, Talalay P (1994) Design and synthesis of bifunctional isothiocyanate analogs of sulforaphane: correlation between structure and potency as inducers of anticarcinogenic detoxication enzymes. J Med Chem. 37: 170–176. PMID: 8289191

4. Shankar S, Ganapathy S, Srivastava RK (2008) Sulforaphane enhances the therapeutic potential of TRAIL in prostate cancer orthotopic model through regulation of apoptosis, metastasis, and angiogenesis. Clin Cancer Res. 14: 6855–6866. doi: 10.1158/1078-0432.CCR-08-0903 PMID: 18980980

5. Fahey JW, Zhang Y, Talalay P (1997) Broccoli sprouts: an exceptionally rich source of inducers of enzymes that protect against chemical carcinogens. Proc Natl Acad Sci. 94: 10367–10372. PMID: 9294217

6. Spitz MR, Duphorne CM, Detry MA, Pillow PC, Amos CI, Lei L, et al. (2000) Dietary intake of isothiocyanates: evidence of a joint effect with glutathione S-transferase polymorphisms in lung cancer risk Cancer Epidemiol. Biomarkers Prev. 9: 1017–1020. PMID: 11045782

7. Zhao H, Lin J, Grossman HB, Hernandez LM, Dinney CP, Wu X (2007) Dietary isothiocyanates, GSTM1, GSTT1, NAT2 polymorphisms and bladder cancer risk. Int J Cancer. 120: 2208–2213. PMID: 17290402

8. Ambrosone CB, McCann SE, Freudenheim JL, Marshall JR, Zhang Y, Shields PG (2004) Breast cancer risk in premenopausal women is inversely associated with consumption of broccoli, a source of isothiocyanates, but is not modified by GST genotype. J Nutr. 134: 1134–1138. PMID: 15113959

9. Joseph MA, Moysich KB, Freudenheim JL, Shields PG, Bowman ED, Zhang Y, et el. (2004) Cruciferous vegetables, genetic polymorphisms in glutathione S-transferases M1 and T1, and prostate cancer risk. Nutr Cancer. 50: 206–213. PMID: 15623468

10. Singh SV, Warin R, Xiao D, Powolny AA, Stan SD, Arlotti JA, et al. (2009) Sulforaphane inhibits prostate carcinogenesis and pulmonary metastasis in TRAMP mice in association with increased cytotoxicity of natural killer cells. Cancer Res. 69: 2117–2125. doi: 10.1158/0008-5472.CAN-08-3502 PMID: 19223537

11. Clarke JD, Dashwood RH, Ho E (2008) Multi-targeted prevention of cancer by sulforaphane. Cancer Lett. 269: 291–304. doi: 10.1016/j.canlet.2008.04.018 PMID: 18504070

12. Zhang Y, Talalay P (1994) Anticarcinogenic activities of organic isothiocyanates: chemistry and mechanisms. J Cancer Res. 54: 1976–1981.

13. Shan Y, Sun C, Zhao X, Wu K, Cassidy A, Bao Y (2006) Effect of sulforaphane on cell growth, G(0)/G(1) phase cell progression and apoptosis in human bladder cancer T24 cells. Int J Oncol. 29: 883–888. PMID: 16964384

14. Herr I, Buchler MW (2010) Dietary constituents of broccoli and other cruciferous vegetables: implications for prevention and therapy of cancer. Cancer Treat Rev. 36: 377–383. doi: 10.1016/j.ctrv.2010.01.002 PMID: 20172656

15. Yu R, Lei W, Mandlekar S, Weber MJ, Der CJ, Wu J, et al. (1999) Role of a mitogen-activated protein kinase pathway in the induction of phase II detoxifying enzymes by chemicals. J Biol Chem. 274: 27545–27552. PMID: 10488090

16. Keum YS, Yu S, Chang PP, Yuan X, Kim JH, Xu C, et al. (2006) Mechanism of action of sulforaphane: inhibition of p38 mitogen-activated protein kinase isoforms contributing to the induction of antioxidant response element-mediated heme oxygenase-1 in human hepatoma HepG2 cells. J Cancer Res. 66: 8804–8813.

17. Juge N, Mithen RF, Traka M (2007) Molecular basis for chemoprevention by sulforaphane: a comprehensive review. J Cell Mol Life Sci. 64: 1105–1127.

18. Nkova-Kostova AT, Talalay P (2008) Direct and indirect antioxidant properties of inducers of cytoprotective proteins. J Mol Nutr Food Res. 52: 128–138.

19. Baldwin AS (2001) Control of oncogenesis and cancer therapy resistance by the transcription factor NF-kappaB. J Clin Invest. 107: 241–246. PMID: 11160144

20. Heiss E, Herhaus C, Klimo K, Bartsch H, Gerhauser C (2001) Nuclear factor kappa B is a molecular target for sulforaphane-mediated anti-inflammatory mechanisms. J Biol Chem. 276: 32008–32015. PMID: 11410599

21. Bryant CS, Kumar S, Chamala S, Shah J, Pal J, Haider M, et al. (2010) Sulforaphane induces cell cycle arrest by protecting RB-E2F-1 complex in epithelial ovarian cancer cells. J Mol Cancer. 9: 47. doi: 10.1186/1476-4598-9-47 PMID: 20196847

22. Corey DR (2007) Chemical Modification: the key to clinical application of RNA interference. J Clin Invest. 117: 3615–3622. PMID: 18060019

23. Giri P, Kumar GS (2008) Self-Structure induction in single stranded poly (A) by small molecules: studies on DNA intercalators, partial intercalators and groove binding molecules. J Arch Biochem Biophys. 474: 183–92. doi: 10.1016/j.abb.2008.03.013 PMID: 18387354

24. N'soukpoe Kossi CN, Desco teaux C, Asselin E, Tajmir- Riahi HA, Be´rube´ G (2008) Transfer RNA bindings to antitumor estradiol-platinum(ii) hybrid and cisplatin. J DNA Cell Biol. 27: 337–343. doi: 10.1089/dna.2008.0727 PMID: 18447754

25. Marmur J, Doty P (1961) Thermal renaturation of deoxyribonucleic acids. J Mol Biol. 3: 585–594. PMID: 14470100

26. Vijalakshmi R, Kanthimathi M, Subramania V (2000) DNA Cleavage by a Chromium (III) Complex. J Biochem Biophys Res Commun. 271: 731–734.

27. Kanakis CD, Tarantilis PA, Polissiou MG, Diamantoglou S, Tajmir-Riahi HA (2005) DNA interaction with naturally occurring antioxidant flavonoids quercetin, kaempferol, and delphinidin. J Biomol Struct Dyn. 22: 719–724. PMID: 15842176

28. Kanakis CD, Tarantilis PA, Polissiou MG, Diamantoglou S, Tajmir-Riahi HA (2007) An overview of DNA and RNA bindings to antioxidant flavonoids. J Cell Biochem Biophys. 49: 29–36.

29. Arakawa H, Ahmad R, Naoui M, Tajmir-Riahi HA (2000) A comparative study of calf thymus DNA binding to Cr (III) and Cr(VI) ions. Evidence for the guanine N-7-chromium-phosphate chelate formation. J Biol Chem. 275: 10150–10153. PMID: 10744697

30. Connors K (1987) Binding Constants: The Measurement of Molecular Complex Stability. Published by John Wiley & Sons, New York.

31. Larsen TA, Goodsell DS, Cascio D, Grzeskowiak K, Dickerson RE (1989) The structure of DAPI bound to DNA. J Biomol Struct Dyn. 7: 477–491. PMID: 2627296

32. Huey R, Morris GM, Olson AJ, Goodsell DS (2007) A semiempirical free energy force field with charge-based desolvation. J Comput Chem. 28: 1145–1152. PMID: 17274016

33. Rappe AK, Casewit CJ, Colwell KS, Goddard WA lll, Skiff WM (1992) UFF, a full periodic table force field for molecular mechanics and molecular dynamics simulations. J Am Chem Soc. 114: 10024–10035.

34. Halgren TA (1996) Merck Molecular Force Field. II. MMFF94 van der Waals and Electrostatic Parameters for Intermolecular Interactions. J Comp Chem. 17: 520–552.

35. Solis FJ, Wets RJB (1981) Minimization by Random Search Techniques. J Math Oper Res. 6: 19–30.

36. Ali HI, Fujita T, Akaho E, Nagamatsu T (2010) A comparative study of AutoDock and PMF scoring performances, and SAR of 2-substituted pyrazolotriazolopyrimidines and 4-substituted pyrazolopyrimidines as potent xanthine oxidase inhibitors. J Comput Aided Mol Des. 24: 57–75. doi: 10.1007/s10822-009-9314-z PMID: 20039101

37. Morris GM, Goodsell DS, Halliday RS, Huey R, Hart WE, Belew RK, et al. (1998) Automated docking using a Lamarckian genetic algorithm and an empirical binding free energy function. J Comput Chem. 19: 1639–1662.

38. Sanner MF (1999) Python: a programming language for software integration and development. J Mol Graph Model. 17: 57–61. PMID: 10660911

39. Couch GS, Hendrix DK, Ferrin TE (2006) Nucleic acid visualization with UCSF Chimera. Nucl Acids Res. 34: 2–5.

40. Alex S, Dupuis P (1989) FT-IR and Raman investigation of cadmium binding by DNA. Inorg Chim Acta. 157: 271–281.

41. Ouameur AA, Tajmir-Riahi HA (2004) Structural analysis of DNA interactions with biogenic polyamines and cobalt (III) hexamine studied by Fourier transform infrared and capillary electrophoresis. J Biol Chem. 279: 42041–42054. PMID: 15284235

42. Nafisi Sh, Manouchehri F, Tajmir-Riahi HA, Varavipour M (2008) Structural features of DNA interaction with caffeine and theophylline. J Mol Struct. 875: 392–399.

43. Nafisi Sh, Adelzadeh M, Norouzi Z, Sarbolouki MN (2009) Curcumin binding to DNA and RNA. DNA Cell Biol. 28: 201–208. doi: 10.1089/dna.2008.0840 PMID: 19364279

44. Ouameur AA, Malonga H, Neault JF, Diamantoglou S, Tajmir- Riahi HA (2004) Taxol interaction with DNA and RNA-stability and structural features. J Chem. 82: 1112–1118.

45. Taillandier E, Liquier J (1992) Infrared spectroscopy of DNA. J Methods Enzymol. 211: 307–335. PMID: 1406313

46. Loprete M, Hartman KA (1993) Conditions for the stability of the B, C and Z structural forms of poly(dG-dC) in the presence of lithium, potassium, magnesium, calcium, and zinc cations. J Biochem. 32: 4077–4082.

47. Tajmir-Riahi HA, Neault JF, Naoui M (1995) Does DNA acid fixation produce lefthanded z structure. J FEBS Lett. 370: 105–108. PMID: 7649286

48. Tajmir-Riahi HA, N'soukpoe´-Kossi CN, Joly D (2009) Structural analysis of protein-DNA and protein-RNA interactions by FTIR, UV–Visible and CD spectroscopic methods. J Spect. 23: 81–101.

49. Polyanichko AM, Andrushchenko VV, Chikhirzhina EV, Vorob'ev VI, Wieser H (2004) The effect of manganese (II) on DNA structure: electronic and vibrational circular dichroism studies. Nucl Acids Res. 32: 989–96. PMID: 14872058

50. Andrushchenko V, Wieser H, Bour P (2002) B-Z conformational transition of nucleic acids monitored by vibrational circular dichroism. Ab initio interpretation of the experiment. J Phys Chem B. 106: 12623–12643.

51. Ouamer AA, Marty R, Neault JF, Tajmir-Riahi HA (2004) AZT binds RNA at multiple sites. J DNA Cell Biol. 23: 783–788. PMID: 15585137